Supporting Information for:

Multi-hydrophilic groups synergistic assembly ionic HOFs with multiple-water clusters and superprotonic single-crystal conductivity

Shu-Hui Li[a], Li-Hui Cao[a,*], Wenmin Zhang[b], Xiang-Tian Bai[a], Xu-Yong Chen[a]

[a] Shaanxi Key Laboratory of Chemical Additives for Industry, College of Chemistry and Chemical Engineering, Shaanxi University of Science and Technology, Xi'an, 710021, China

[b] Department of Chemical Engineering and Food Science, Zhengzhou University of Technology, Zhengzhou 450044 Henan Province, China

[*]Corresponding author.

E-mail: caolihui@sust.edu.cn

Section S1. Materials and characterization.

1. Materials methods and experimental details.

Materials and reagents. 4-amino benzonitrile, CsF, 4-Fluorobenzonitrile, N, N-Dimethylformamide (DMF), tetrahydrofuran (THF), lithium bis (trimethylsilyl) azanide (LiHMDS), ethanol (EtOH), hydrochloric acid (HCl), 3,6-dihydroxy -2,7-naphthalenedisulfonic acid disodium salt (DHNDS), 4,4',4"4"'-methanetetrayltetrabenzimidamide (TAM). All the chemicals above were bought from commercial vendors and used without further purification.

The 4,4',4"-nitrilotribenzimidamide (TTMM) synthesis was synthesized according to previous report[1,2] with slight modification.

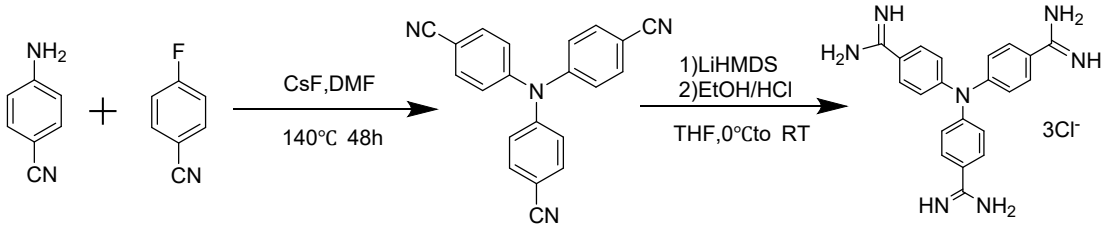

SchemeS1. Schematic representation of ligand formation reaction.

1.18 g (10 mmol) of 4-aminobenzonitrile was dissolved in 50 mL dry DMF. Then 6.04 g (40 mmol) of CsF was added slowly to the solution with continuous stirring followed by the addition of 2.66 g (22 mmol) of 4-Fluorobenzonitrile. The total reaction mixture was then refluxed at 140 ºC for 48 hours. After cooling, the reaction mixture was poured into ice-cold water to precipitate out the product (4,4′,4″-tricyanotriphenylamine). The precipitate was filtered and washed with plenty of water and finally dried in a hot air oven to yield 2.57 g (79%) of 4,4′,4″-tricyanotriphenylamine.

In the second step. 4,4′,4″-tricyanotriphenylamine (5 g, 15.6 mmol) was dissolved in dry THF (92 mL). It was cooled to -78 ℃ under a nitrogen atmosphere, and LiHMDS solution (80 mL) was added resulting in the immediate formation of a precipitate. The mixture was allowed to warm to room temperature and stirred overnight, during which time the precipitate dissolved to give a yellow-orange solution.

This was cooled to 0 ℃ and ethanolic HCl (prepared by cautiously adding 12.7 mL of acetyl chloride to 64 mL ethanol) was added, which resulted in the formation of a pale precipitate and sonicated for 1 hour. Filtration to obtain a solid was washed thoroughly with ethanol (300 mL) and dried in vacuo to give TTMM as a cream-colored powder. Yield: 7.44 g (96%).

Synthesis of iHOF-43. DHNDS (6 mg, 0.016 mmol) was completely dissolved in water (1.5 mL). Simultaneously TTMM (6 mg, 0.016 mmol) was stirred until completely dissolved in methanol (1.5 mL). The two clarified solutions were then mixed and left in a clean and cool place for one week to obtain yellowish-green transparent crystals in the yield of: 67%.

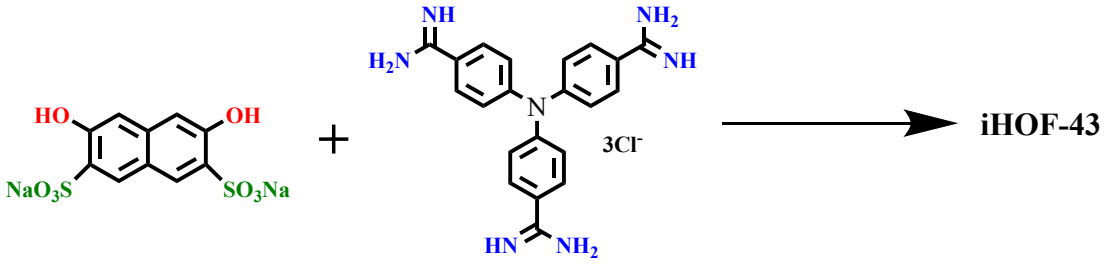

Scheme S2. Schematic representation for preparation of compound **iHOF-43**.

Synthesis of iHOF-44. Water (4 mL) was added to DHNDS (7.29 mg, 0.020 mmol) and TAM (6.34 mg, 0.013 mmol) was added to water (4 mL). The two clear solutions were then mixed and left at room temperature for 3-5 days. Long yellowish crystals grow gradually. The yield was 64%.

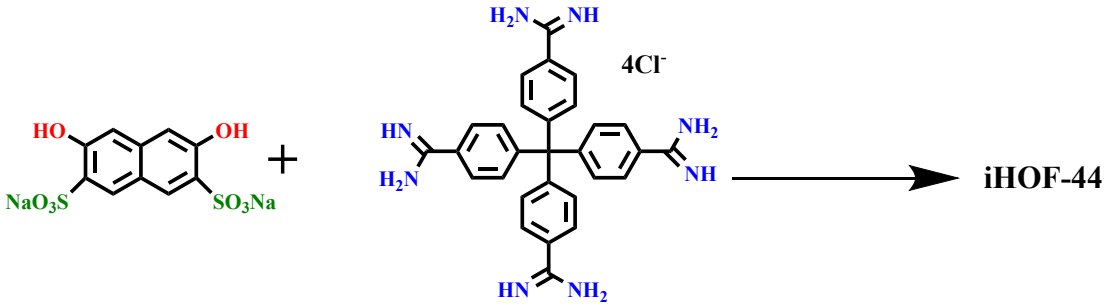

Scheme S3. Schematic representation for preparation of compound **iHOF-44**.

2. Instrumentation.

Powder x-ray diffraction (PXRD) was measured on a *Bruker MXIμS microsource* (*Mo - kα radiation*) and an *Apex II CCD* detector in the range of 2θ = 3.0-60.0º. 1H NMR spectra were performed on a Bruker-400 MHz NMR spectrometer. Thermogravimetric analysis (TGA) measurements were carried out on a TGA-55 instrument at temperatures ranging from room temperature to 800 ºC with a heating rate of 10 ºC·min^{-1}. Fourier-transform infrared (FT-IR) spectra were obtained on a Bruker VECTOR-22 FTIR spectrometer in the 4000~400 cm^{-1} region with KBr pellets.

3. Measurements of proton conductivity.

The procedure for preparing samples for testing proton conductivity is as follows: The microcrystalline **iHOF-43** and **iHOF-44** samples were subjected to 10.00 MPa pressure to form microcrystalline particles with a diameter of 7 mm and a thickness of 1.0 - 1.6 mm, and the particles were sandwiched between two copper plates for testing. Measuring the **iHOF-43** single crystal, the large size single crystal was cut into a uniform cuboid with a scalpel. The conductive silver glue was connected with a silver wire to test its conductivity along the *a*-axis direction. To test the conductivity in the *b*-axis and *c*-axis directions, a single crystal is cut into a uniform rectangular shape. Their thickness, diameter, and length are measured by vernier calipers. Impedance analysis was performed using an electrochemical workstation (CHI 660E) in the frequency range of 1 Hz to 0.1 MHz. Temperature and relative humidity were controlled by a high and low temperature and humidity chamber. The proton conductivity is calculated as follows: $\sigma = L/RS$, where σ is the proton conductivity (S·cm^{-1}), L is the distance between two copper sheets or two silver wires (cm), R is the electrochemical impedance value, and S is the surface area of the sample in contact with the copper sheet or silver wire (cm^2).

With a two-electrode AC impedance spectrum at an AC voltage of 5 mV. Temperature and humidity were controlled using a high and low temperature and humidity test chamber. After 50 minutes of equilibration, the impedance values were repeated at each temperature until the measured values remained constant. The

impedance profiles were fitted by *ZView*[2] software to obtain the resistance values. The equivalent circuit used for the assembly is as follows:

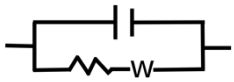

C(RW)

The value of activation energy E_a was calculated according to the Arrhenius equation: $T\sigma = \sigma_0 \exp(-E_a/kT)$, where σ_0 is the Prefinger factor, T is the temperature, and k is the Boltzmann constant.

4. Single crystal X-ray diffraction analyses.

Single-crystal X-ray diffraction data for the **iHOF-43** and **iHOF-44** compounds were collected on a *Bruker SMART APEX CCDC* diffractometer equipped with graphite monochromatic Cu-Kα radiation (λ = 0.71073 Å) using the ω scanning technique. The data were reduced using SAINT and corrected for Lorentzian and polarization effects. Adsorption corrections were performed using the *SADABS* program.[3] All structures were solved by direct methods (*SHELXS*) and full matrix least-squares refinement was performed using *OLEX2*[4] on F^2 using the *SHELXL-2015* module.[5] Displacement parameter constraints were used for ligand modeling. Where possible, hydrogen atoms were geometrically placed on their lapping atoms. Tables S1 and Tables S2 summarize the crystal data for the title complex, including space groups, lattice parameters, and other relevant information. For more details on the crystal data, see the X-ray crystal file in CIF format. Full details of the structure determination have been deposited at the Cambridge Crystallographic Data Center, **iHOF-43** reference number CCDC 2406278 and **iHOF-44** reference number CCDC 2406277, and are available free of charge from CCDC.

Section S2: Crystal data and structure.

Table S1. Crystal structure data and refinement details of **iHOF-43**.

Compounds	iHOF-43
Empirical formula	$C_{144}H_{258}N_{28}O_{112}S_{12}$
Formula weight	4558.49
Temperature / K	100.01(10)
Crystal system	triclinic
Space group	*P*-1
a/Å	15.89692(19)
b/Å	24.3336(3)
c/Å	31.3004(4)
α/°	82.4312(11)
β/°	76.3819(11)
γ/°	78.0115(11)
Volume/Å^3	11467.1(3)
Z	2
ρ_{calc} g/cm^3	1.3201.947
μ/mm^{-1}	1.947
F (000)	4812.0
Radiation	Cu Kα (λ = 1.54184)
2Θ range for data collection/°	4.528 to 151.914
Index ranges	-18 ≤ h ≤ 19, -30 ≤ k ≤ 30, -39 ≤ l ≤ 39
Reflections collected	137872
Independent reflections	46475 [R_{int} = 0.0657, R_{sigma} = 0.0596]
Data/restraints/parameters	46475/15/2882
Goodness-of-fit on F^2	2.320
Final R indexes [I>=2σ (I)]	R1 = 0.1938, wR2 = 0.5088
Final R indexes [all data]	R1 = 0.2090, wR2 = 0.5198
Largest diff. peak and hole / e. Å^{-3}	0.10/-0.03
CCDC number	2406278

$^aR_1 = \text{å}||F_o|-|F_c||/\text{å}|F_o|$. $^bwR_2 = \{\text{å}[w(F_o^2-F_c^2)^2]/\text{å}[w(F_o^2)^2]\}^{1/2}$

Table S2. Crystal structure data and refinement details of **iHOF-44**.

Compounds	**iHOF-44**
Empirical formula	$C_{98}H_{166}N_{16}O_{71}S_8$
Formula weight	2960.94
Temperature / K	150(2)
Crystal system	triclinic
Space group	*P*-1
a/Å	13.8167(5)
b/Å	16.0738(6)
c/Å	32.1757(12)
α/°	102.8797(19)
β/°	95.113(2)
γ/°	95.376(2)
Volume/Å^3	6890.7(4)
Z	2
ρ_{calc} g/cm^3	1.427
μ/mm^{-1}	2.120
F (000)	3124.0
Radiation	CuKα (λ = 1.54178)
2Θ range for data collection/°	5.672 to 149.624
Index ranges	-17 ≤ h ≤ 17, -20 ≤ k ≤ 18, -40 ≤ l ≤ 40
Reflections collected	97888
Independent reflections	28158 [Rint = 0.0691, Rsigma = 0.0908]
Data/restraints/parameters	28158/206/1898
Goodness-of-fit on F^2	1.040
Final R indexes [I>=2σ (I)]	R1 = 0.0809, wR2 = 0.2190
Final R indexes [all data]	R1 = 0.0947, wR2 = 0.2404
Largest diff. peak and hole / e. Å^{-3}	0.93/-0.55
CCDC number	2406277

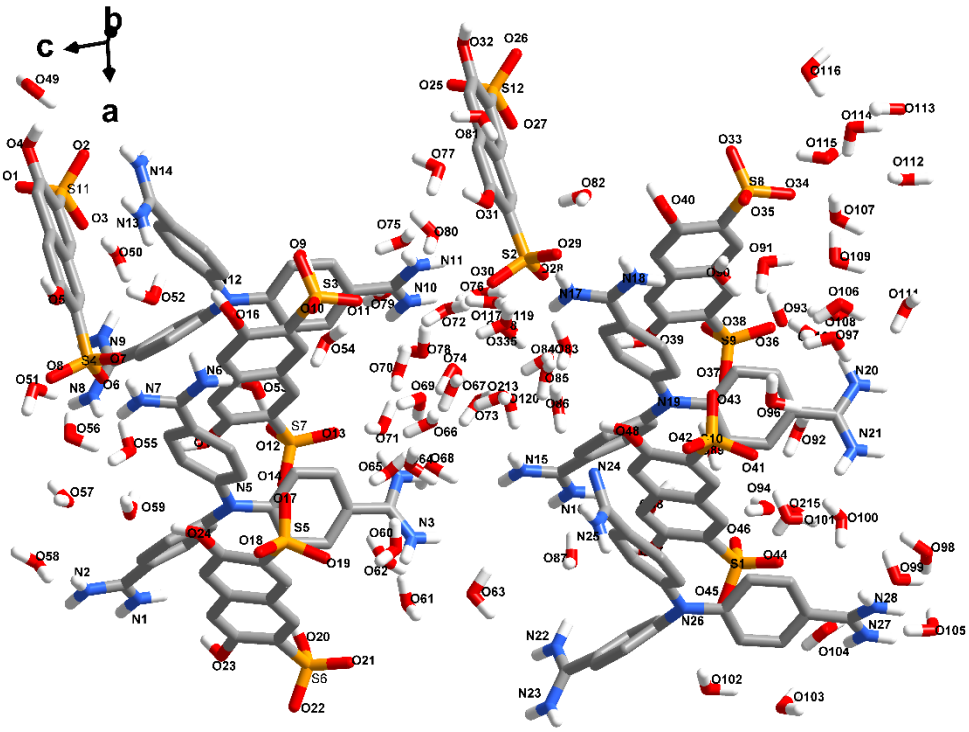

Figure S1. Asymmetric unit of **iHOF-43**.

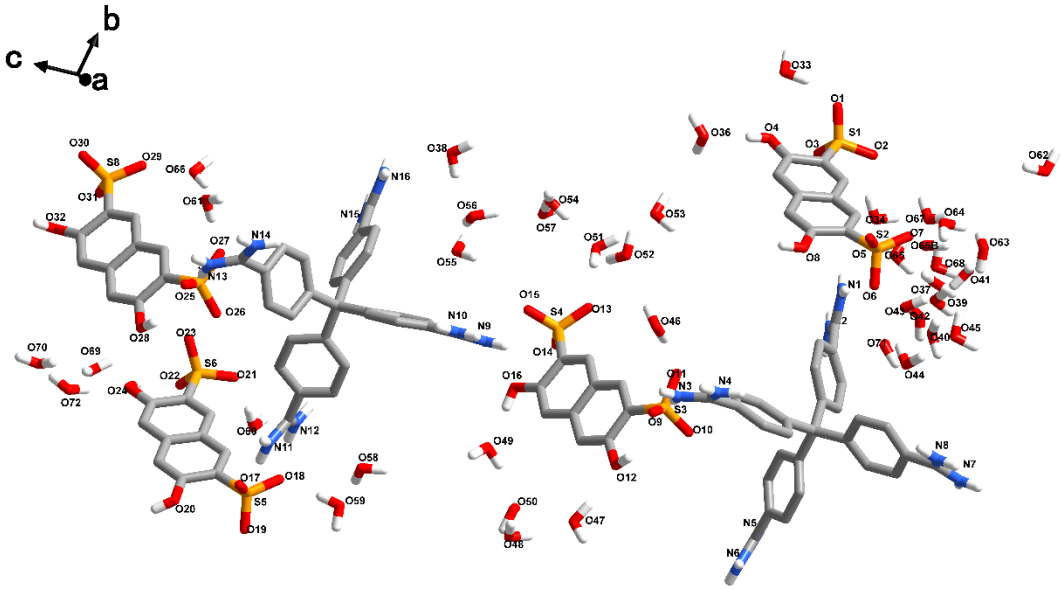

Figure S2. Asymmetric unit of **iHOF-44**.

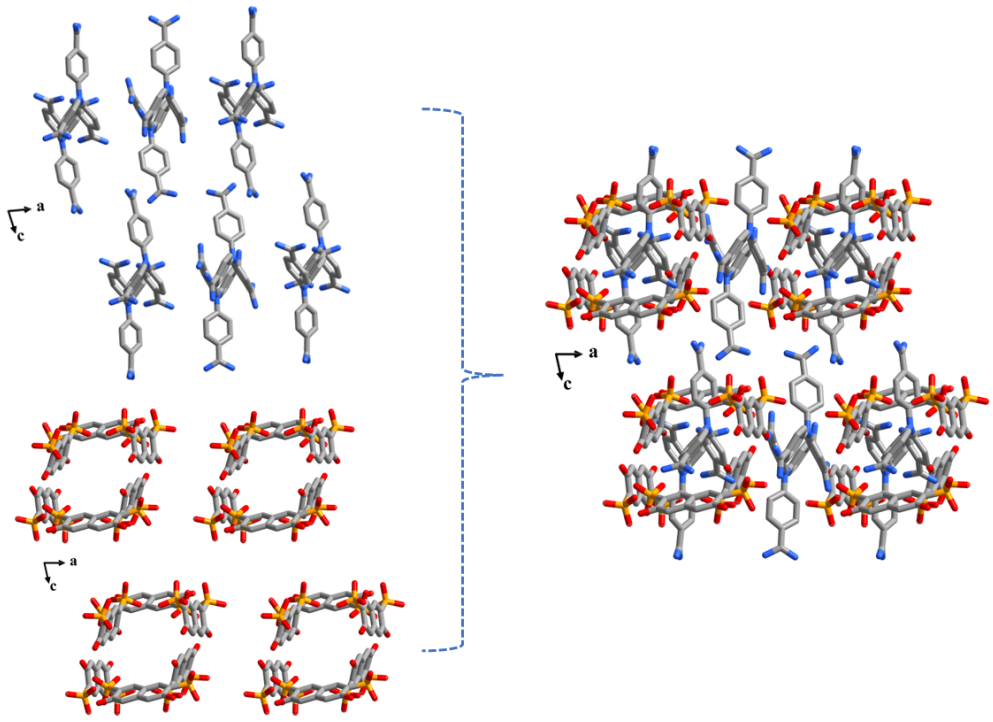

Figure S3. Amidine and sulfonic acid framework in the supramolecular structure of **iHOF-43.**

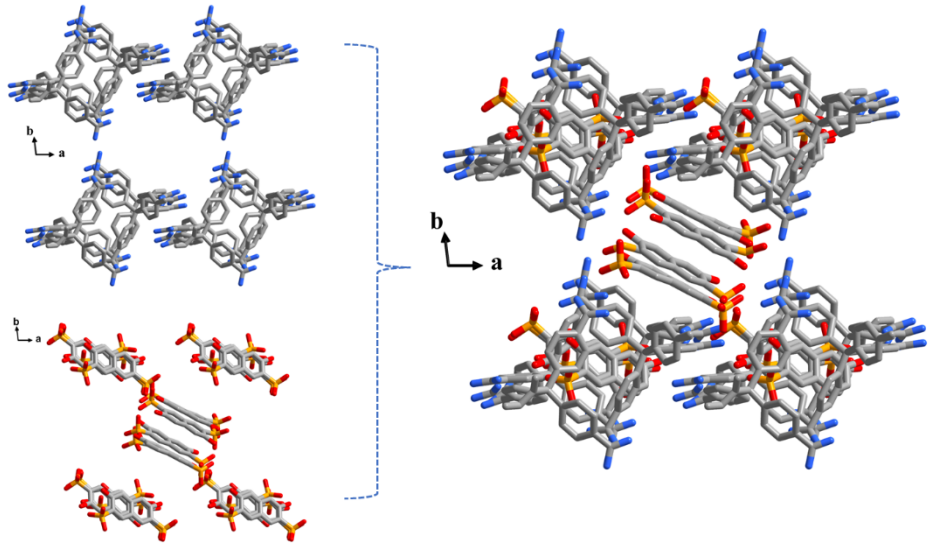

Figure S4. Amidine and sulfonic acid framework in the supramolecular structure of **iHOF-44.**

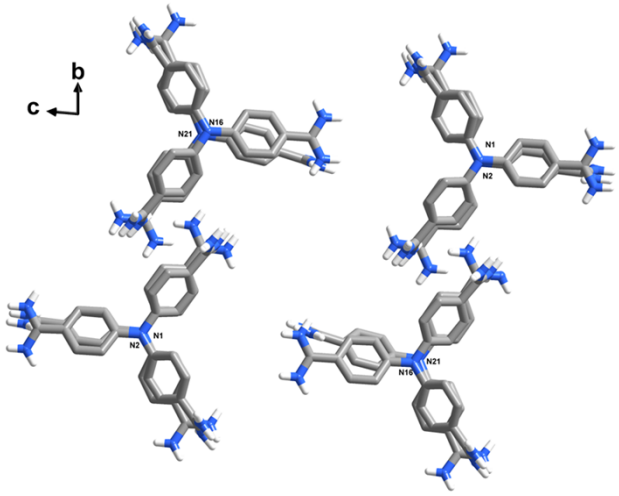

Figure S5. Four TTMM stacking structures in **iHOF-43.**

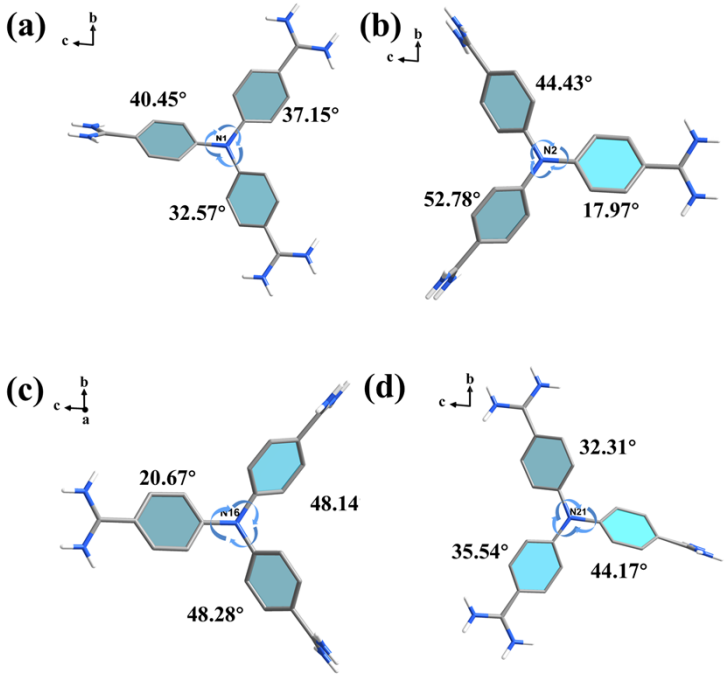

Figure S6. (a) The rotated dihedral angle diagram of **N1** in TTMM using the plane formed by C on the three benzene rings attached to **N1** as the reference plane. **(b)** The rotated dihedral angle diagram of **N2** in TTMM using the plane formed by C on the three benzene rings attached to **N2** as the reference plane. **(c)** The rotated dihedral angle diagram of **N16** in TTMM using the plane formed by C on the three benzene rings attached to **N16** as the reference plane. **(d)** The rotated dihedral angle diagram of **N21** in TTMM using the plane formed by C on the three benzene rings attached to **N21** as the reference plane.

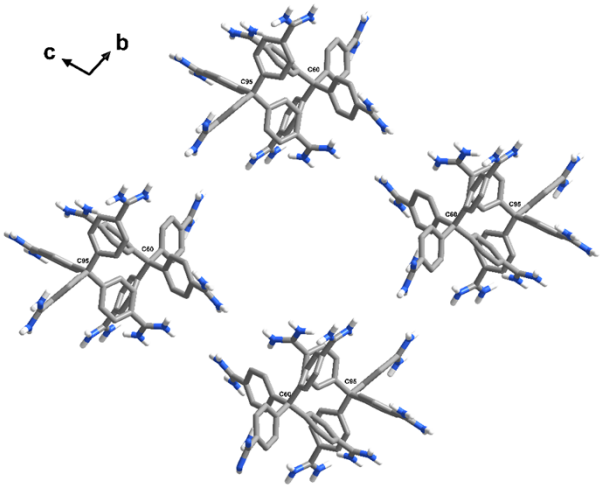

Figure S7. Two TAM stacking structures in **iHOF-44**.

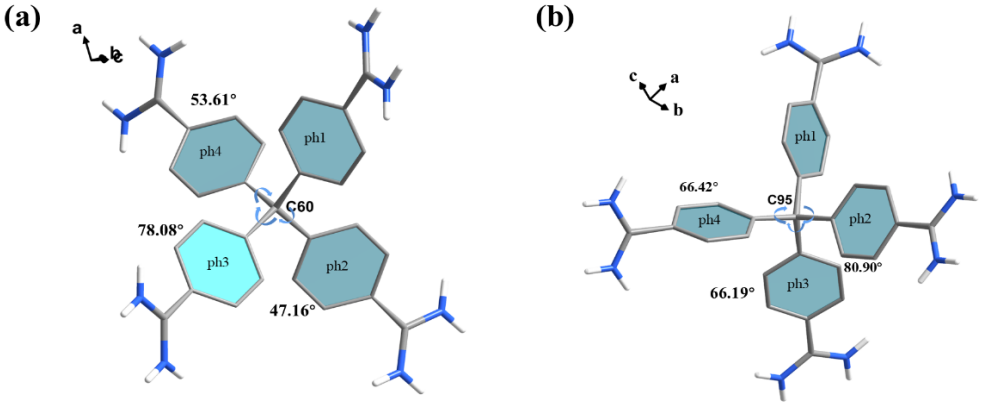

Figure S8. (a) Rotated dihedral angle diagram of **TAM-C60** with ph1 as a reference plane. **(b)** Rotated dihedral angle diagram of **TAM-C95** with ph1 as the reference plane.

Section S3: Optical image and digital images.

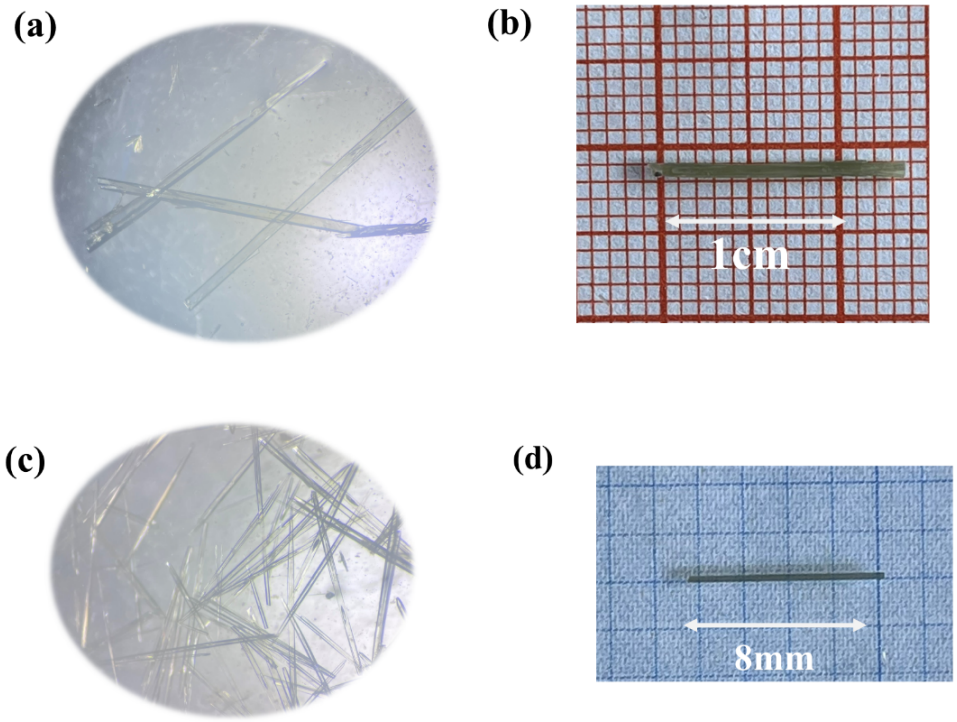

Figure S9. (a) Optical image of **iHOF-43** crystals. **(b)** Digital images of **iHOF-43** crystals. **(c)** Optical image of **iHOF-44** crystals. **(d)** Digital images of **iHOF-44** crystals.

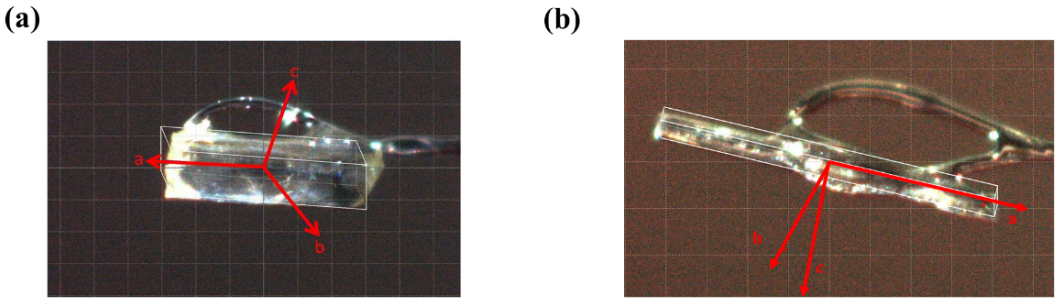

Figure S10. (a) Single crystal **iHOF-43** on the X-ray diffractometer and the diffractions corresponding to each axis of the crystal. **(b)** Single crystal **iHOF-44** on the X-ray diffractometer and the diffractions corresponding to each axis of the crystal.

Section S4: ^{1}H NMR spectra and ^{13}C NMR spectrum.

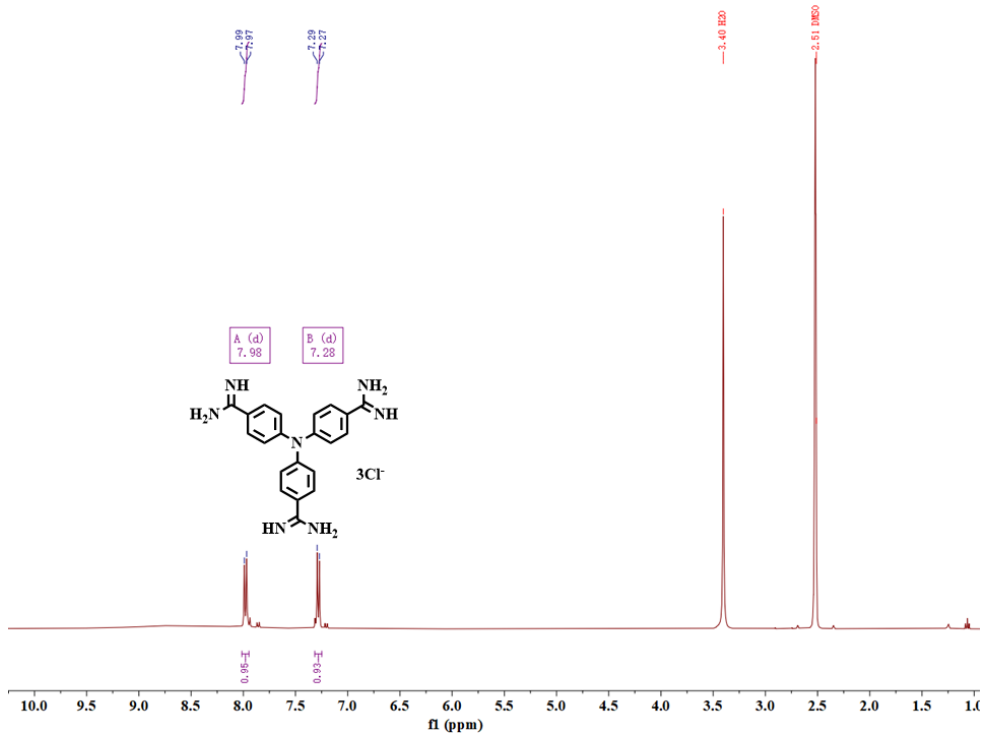

Figure S11. ^{1}H NMR spectrum of TTMM (DMSO-d_6, 400 MH_Z).

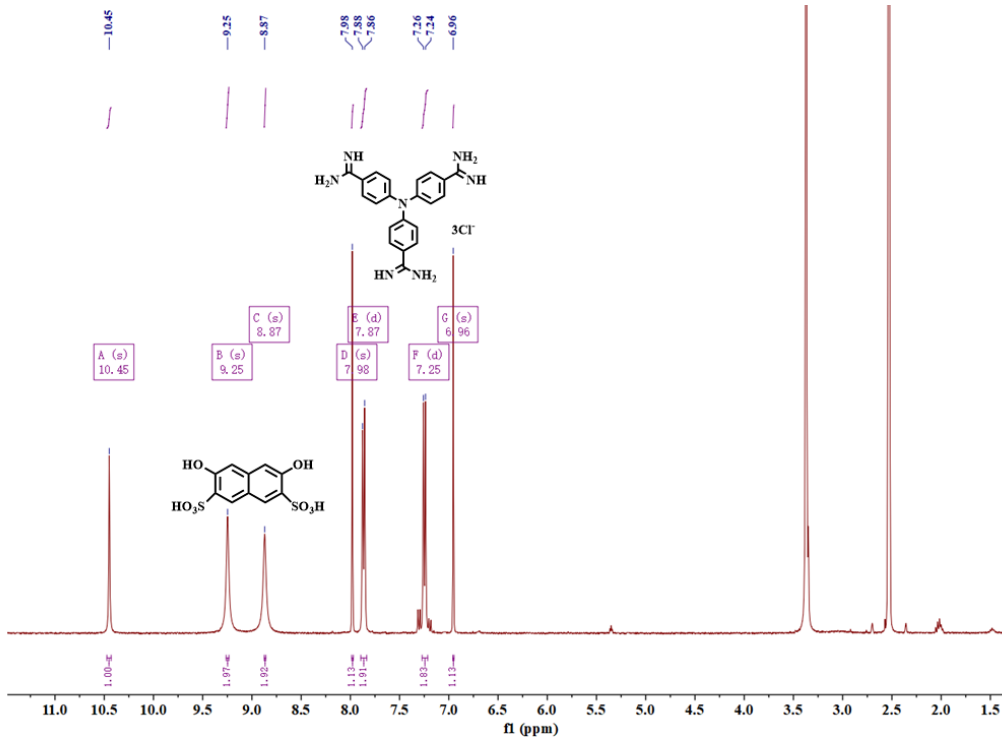

Figure S12. ^{1}H NMR spectrum of **iHOF-43** (DMSO-d_6, 400 MH_Z).

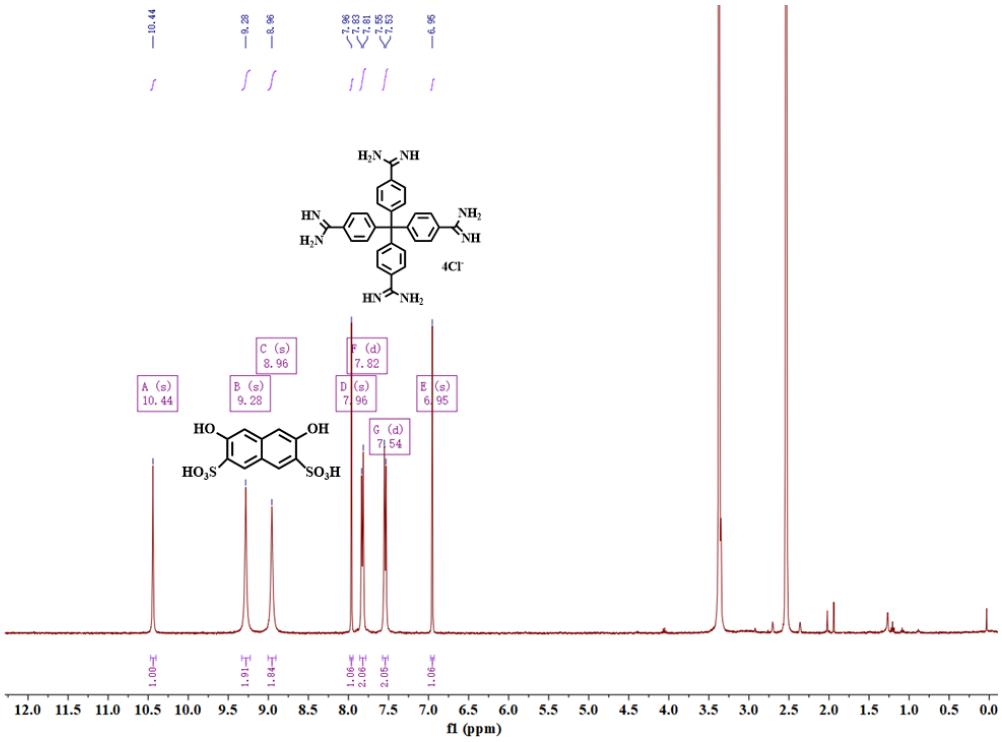

Figure S13. ^{1}H NMR spectrum of **iHOF-44** (DMSO-d_6, 400 MH_Z).

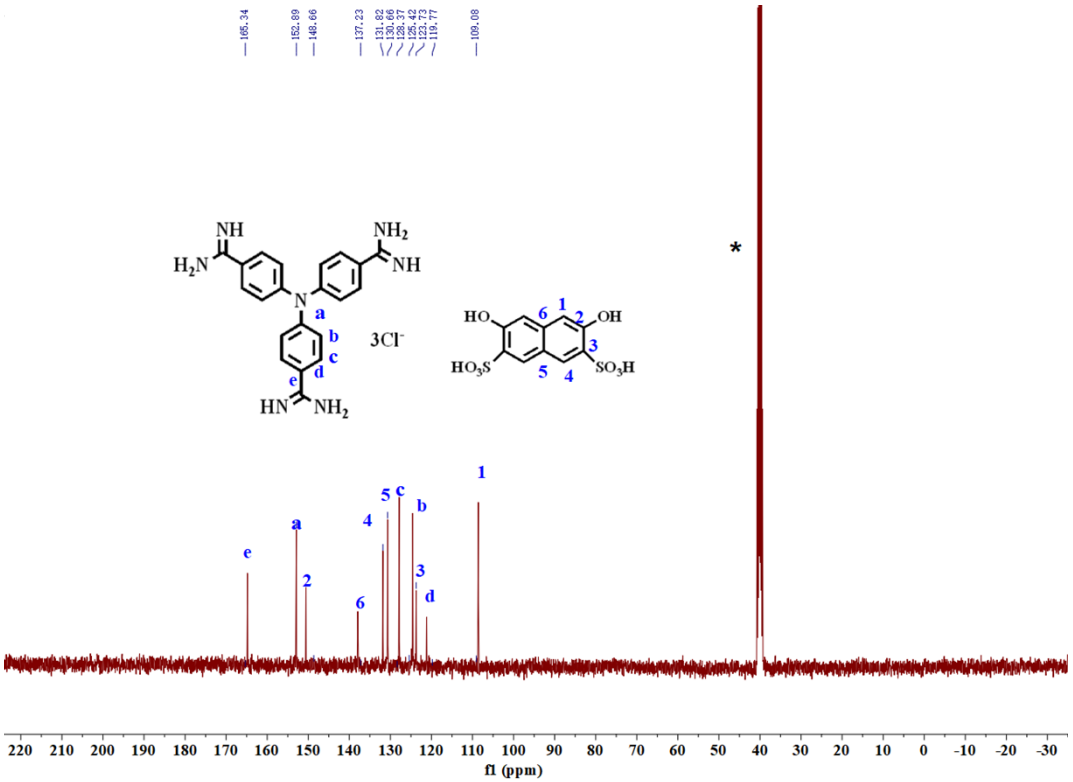

Figure S14. ^{13}C NMR spectrum of **iHOF-43** (400 MHz, 298 K, d6-DMSO, peak marked * corresponds to residual solvent signal).

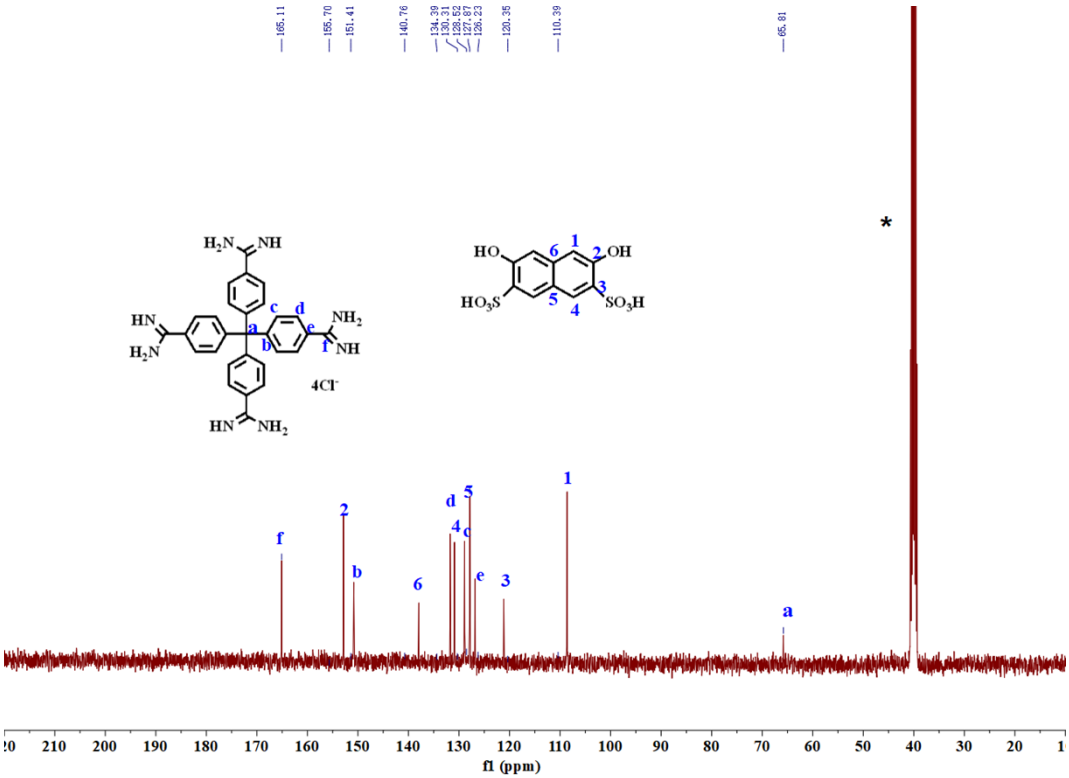

Figure S15. ^{13}C NMR spectrum of **iHOF-44** (400 MHz, 298 K, d6-DMSO, peak marked * corresponds to residual solvent signal).

Section S5: Thermal stability.

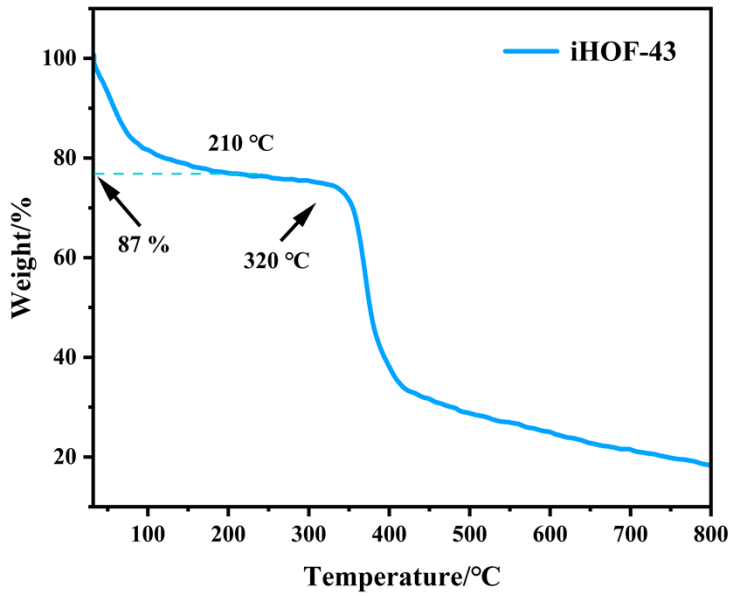

Figure S16. TGA plots of **iHOF-43.**

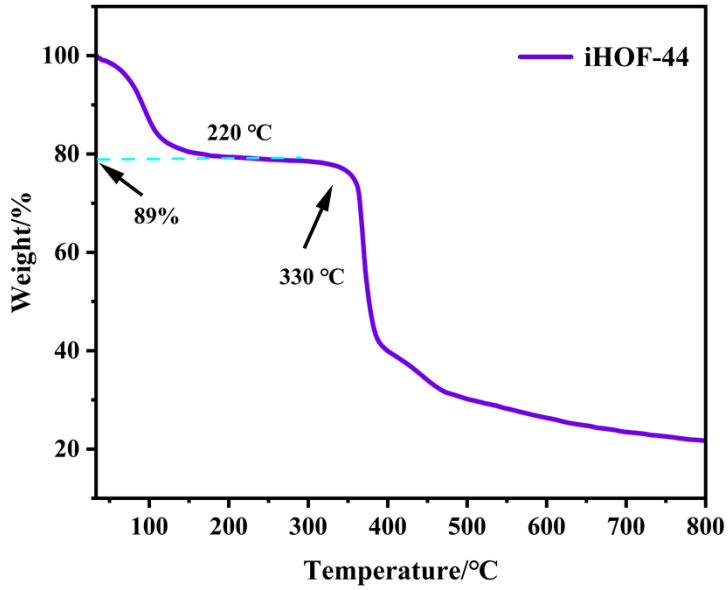

Figure S17. TGA plots of **iHOF-44.**

Section S6: FT-IR analysis.

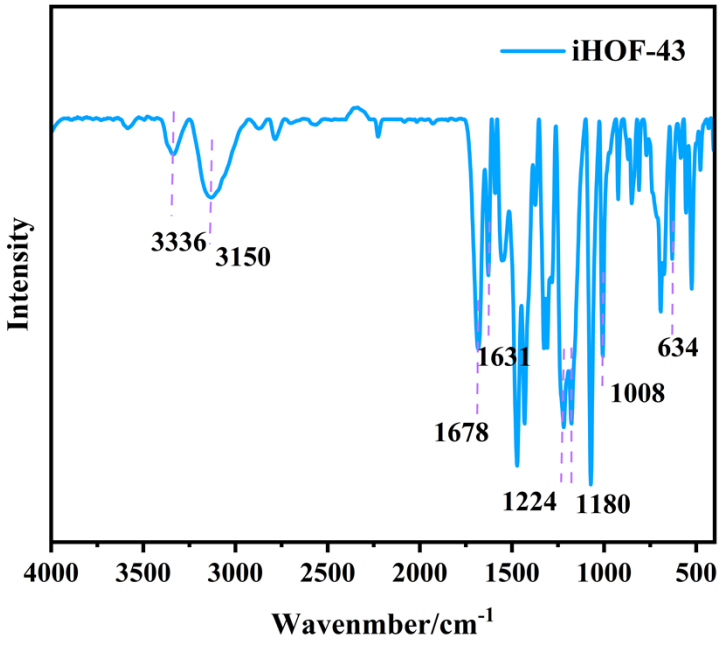

Figure S18. FT-IR of **iHOF-43.**

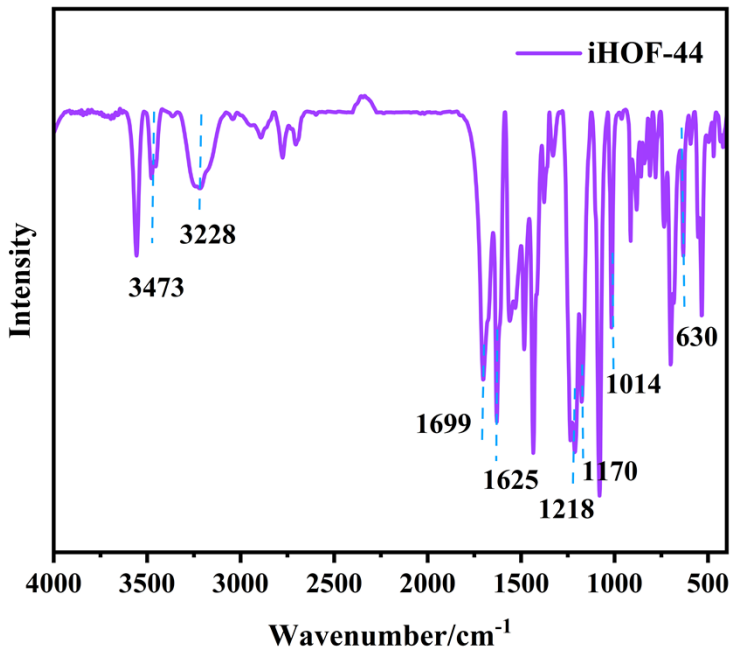

Figure S19. FT-IR of **iHOF-44.**

Section S7. Proton conductivity of iHOF-43.

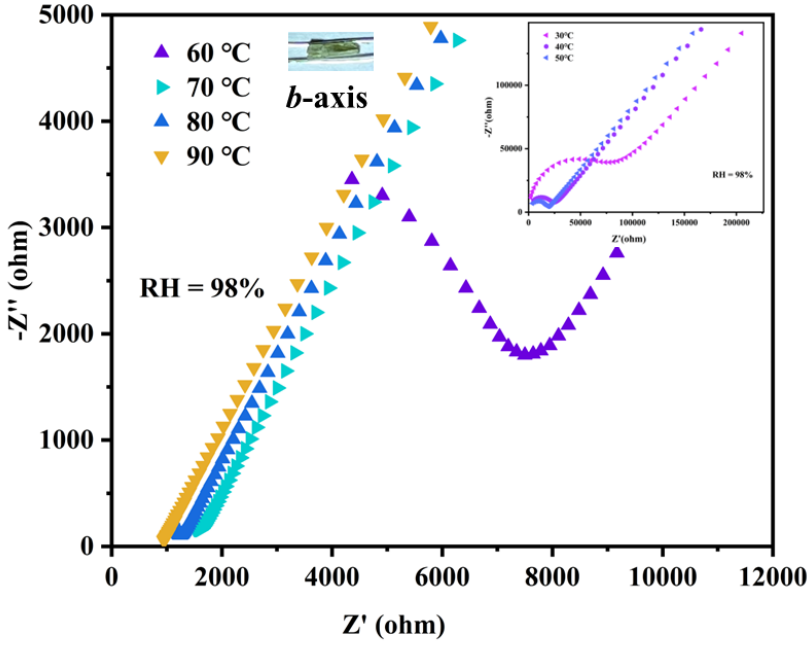

Figure S20. The **iHOF-43** single crystal conductivity test results at 98% RH along the ***b*-axis** direction.

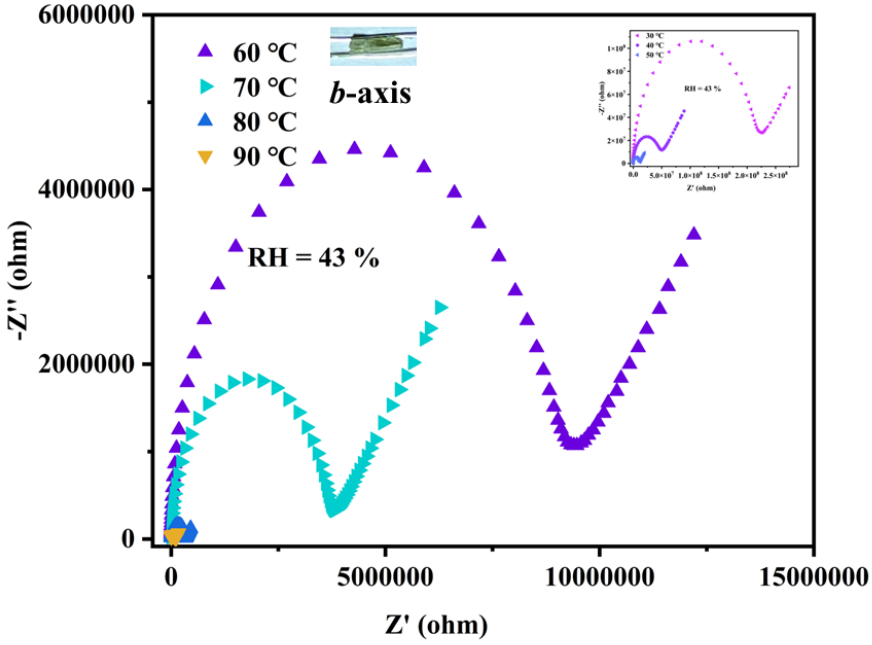

Figure S21. The **iHOF-43** single crystal conductivity test results at 43% RH along the ***b*-axis** direction.

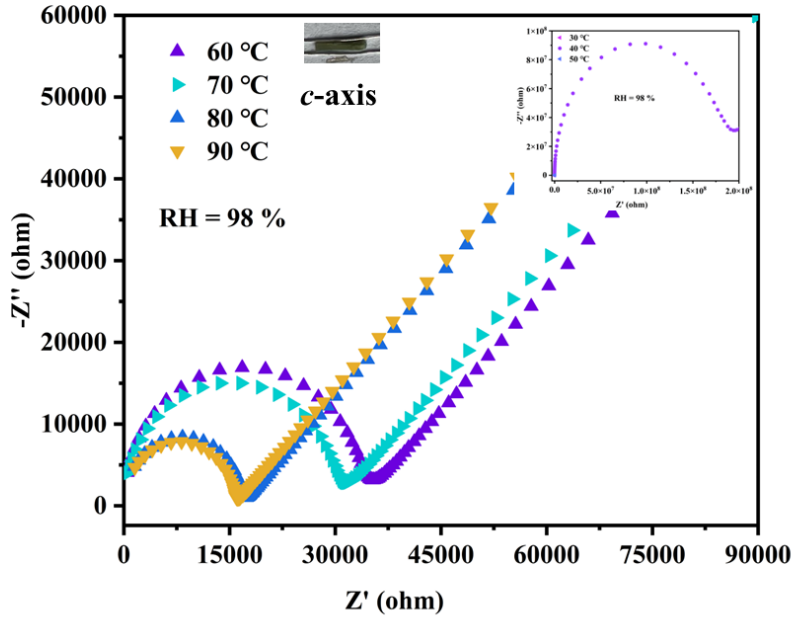

Figure S22. The **iHOF-43** single crystal conductivity test results at 98% RH along the ***c*-axis** direction.

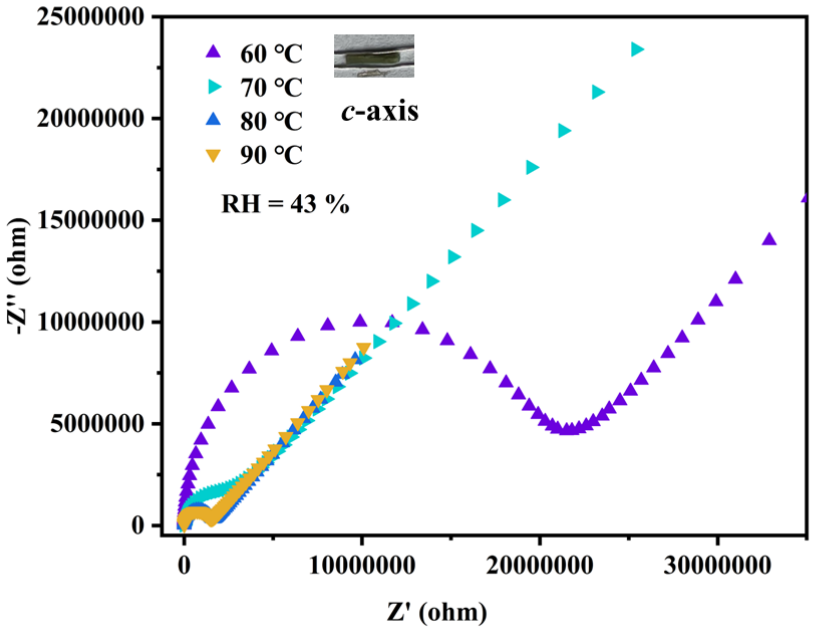

Figure S23. The **iHOF-43** single crystal conductivity test results at 43% RH along the ***c*-axis** direction.

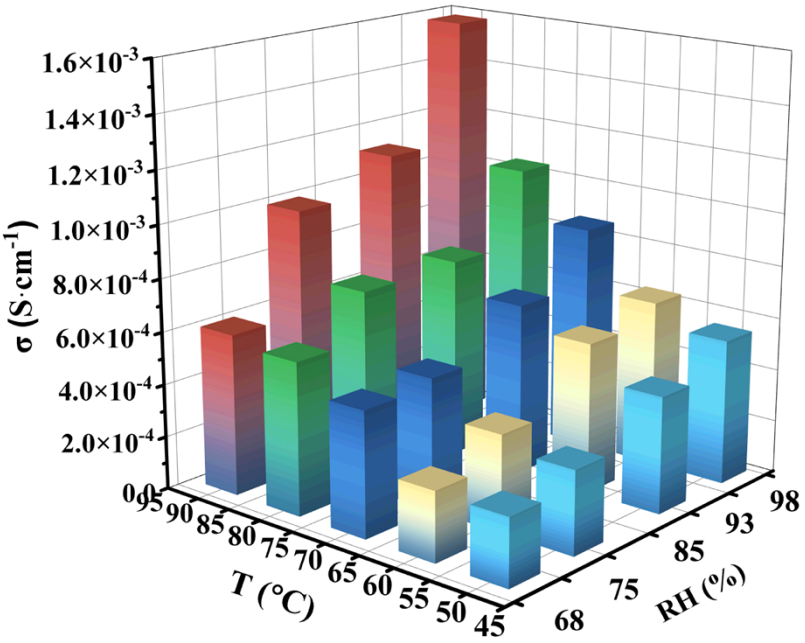

Figure S24. The **iHOF-43** single crystal conductivity test results along the ***b*-axis** direction at different RH.

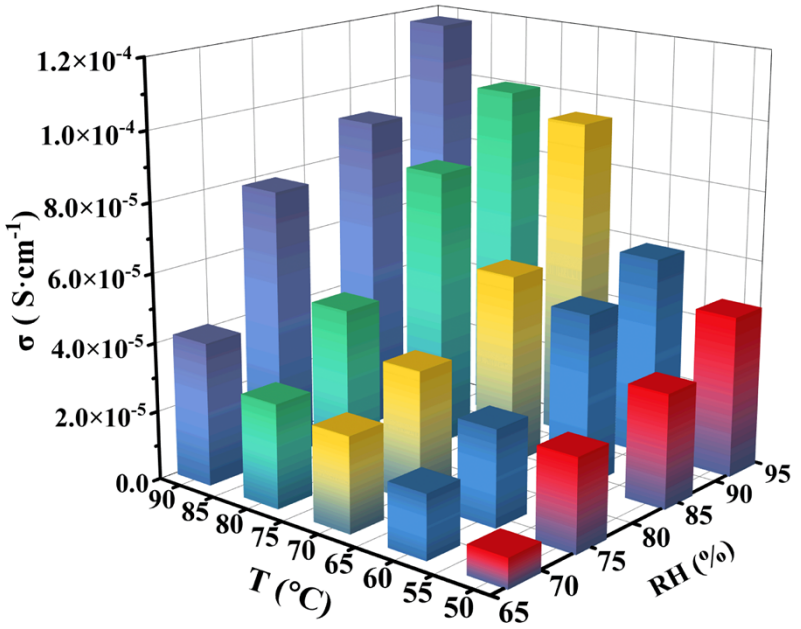

Figure S25. The **iHOF-43** single crystal conductivity test results along the ***c*-axis** direction at different RH.

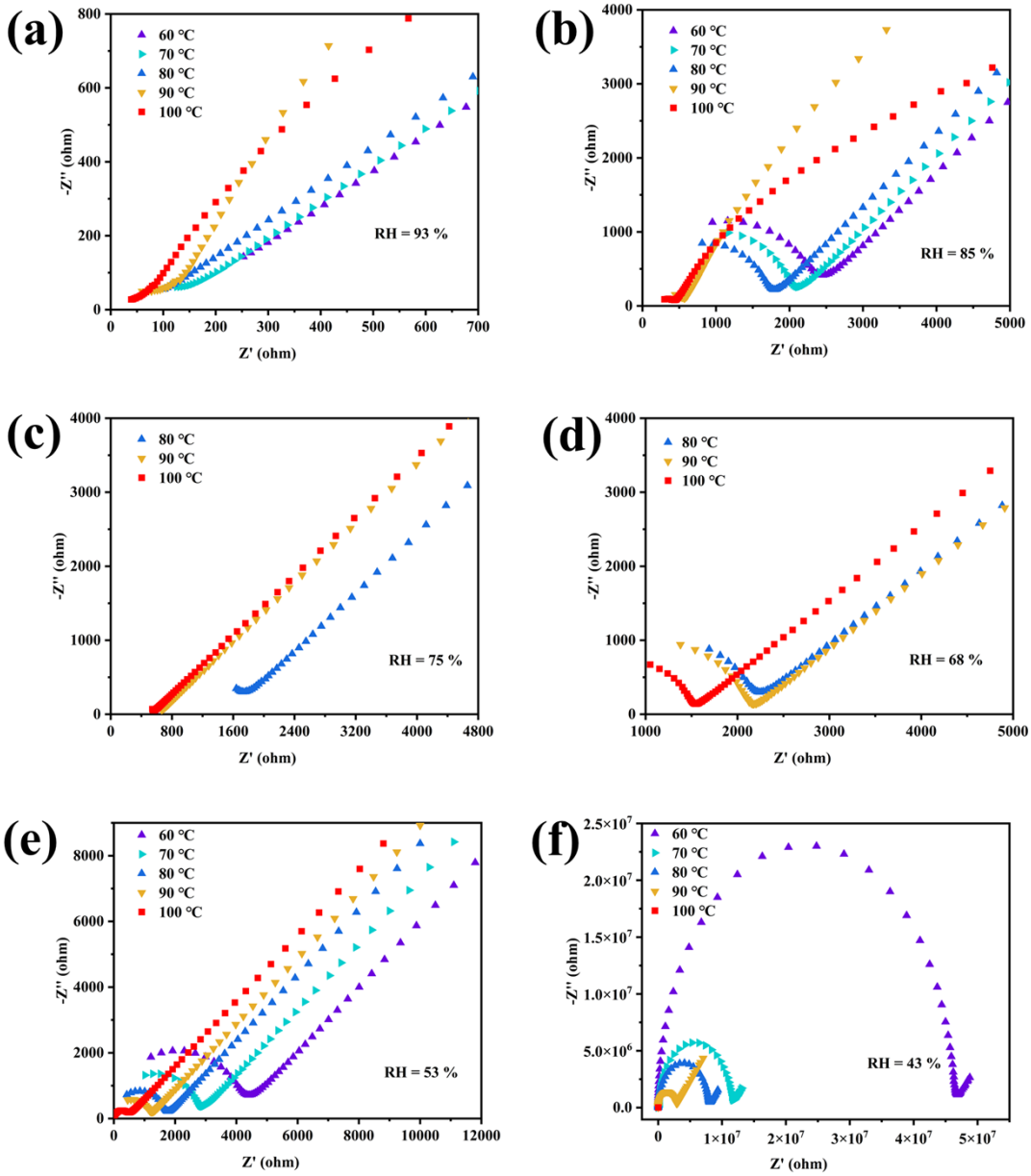

Figure S26. Nyquist plots of conductivity test results of **iHOF-43** pellet at different RH, **(a)** 93% RH, **(b)** 85% RH, **(c)** 75% RH, **(d)** 68% RH, **(e)** 53% RH, **(f)** 43% RH.

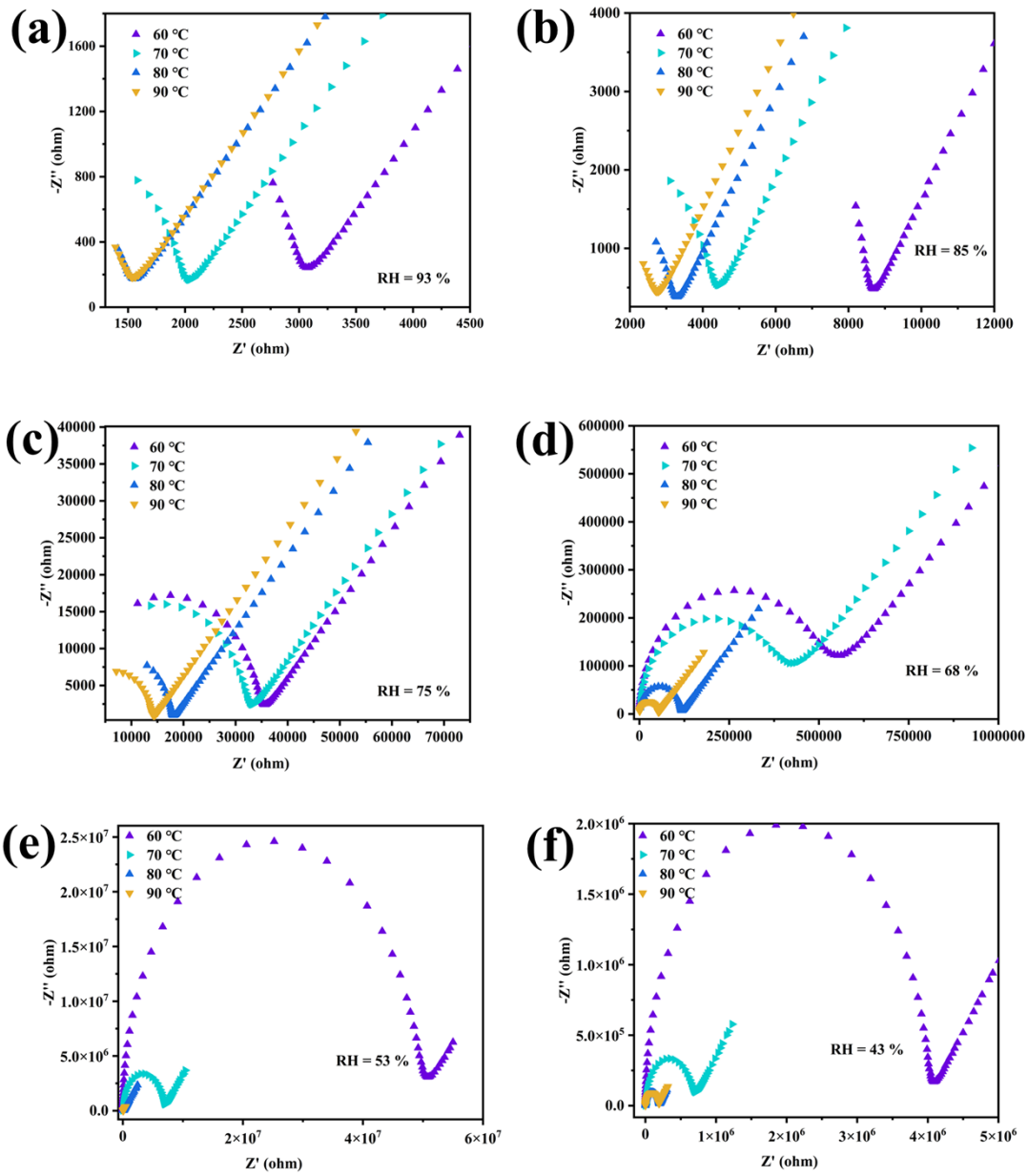

Figure S27. The **iHOF-43** single crystal conductivity test results along the ***a*-axis** direction at different RH, **(a)** 93% RH, **(b)** 85% RH, **(c)** 75% RH, **(d)** 68% RH, **(e)** 53% RH, **(f)** 43% RH.

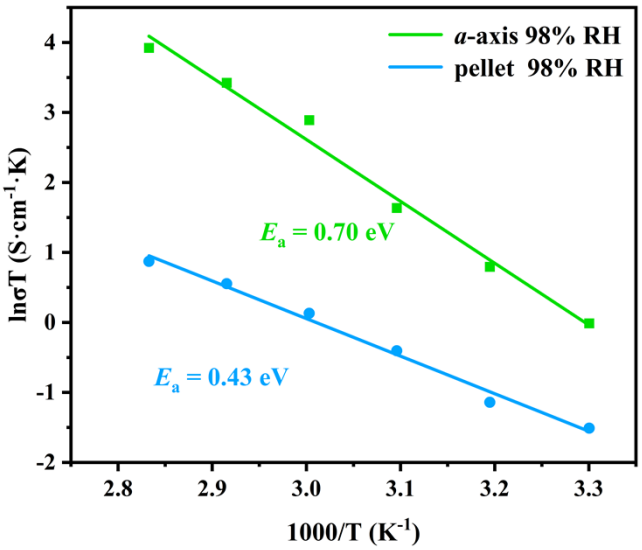

Figure S28. Arrhenius diagram of **iHOF-43** pellet and single crystal along the *a*-axis at 98% RH.

Section S8. Proton conductivity of iHOF-44.

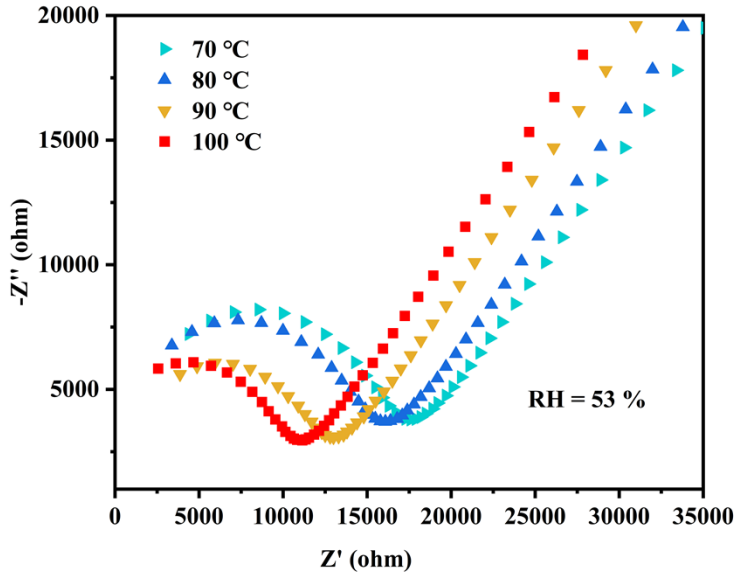

Figure S29. The **iHOF-44** powder conductivity test results at 53% RH.

Table S3. Proton conductivities ($S \cdot cm^{-1}$) for **iHOF-44** powder at 50-100 ºC and different Relative humidity (RH).

pellet	50 °C	60 °C	70 °C	80 °C	90 °C	100 °C
53%	8.13×10^{-6}	1.01×10^{-5}	2.16×10^{-5}	2.40×10^{-5}	2.98×10^{-5}	3.48×10^{-5}
68%	4.08×10^{-5}	6.62×10^{-5}	1.80×10^{-4}	2.03×10^{-4}	2.31×10^{-4}	3.23×10^{-4}
75%	5.29×10^{-5}	8.74×10^{-5}	1.92×10^{-4}	2.15×10^{-4}	2.67×10^{-4}	4.87×10^{-4}
85%	7.68×10^{-5}	9.31×10^{-5}	2.10×10^{-4}	2.48×10^{-4}	3.53×10^{-4}	5.68×10^{-4}
93%	8.06×10^{-5}	4.27×10^{-4}	4.41×10^{-4}	4.79×10^{-4}	6.42×10^{-4}	7.39×10^{-4}
98%	2.25×10^{-4}	5.12×10^{-4}	7.85×10^{-4}	1.06×10^{-3}	2.50×10^{-3}	2.71×10^{-3}

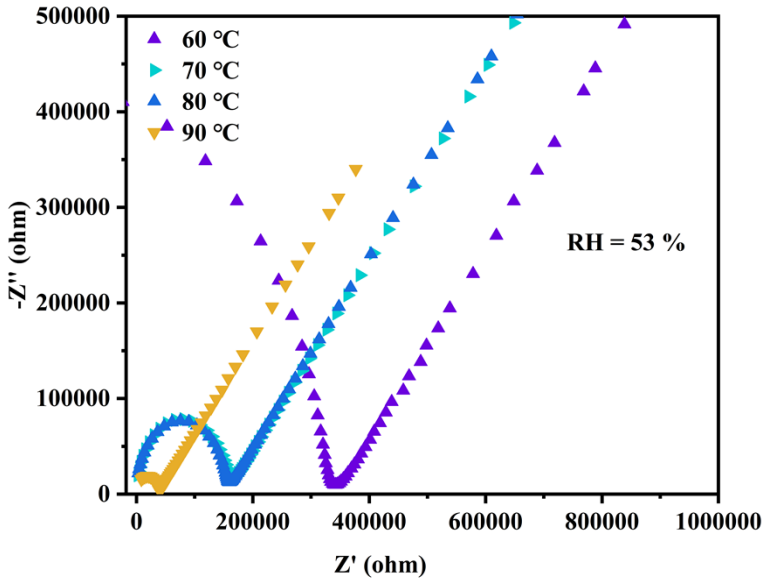

Figure S30. The **iHOF-44** single crystal conductivity test results along the ***a*-axis** direction at 53% RH.

Table S4. Proton conductivities ($S \cdot cm^{-1}$) for **iHOF-44** single crystal along the *a*-axis direction at 50-90 ℃ and different Relative humidity (RH).

***a*-axis**	**50 ℃**	**60 ℃**	**70 ℃**	**80 ℃**	**90 ℃**
53%	1.47×10^{-4}	4.04×10^{-4}	8.33×10^{-4}	8.58×10^{-4}	3.46×10^{-3}
68%	4.08×10^{-4}	1.02×10^{-3}	2.10×10^{-3}	2.93×10^{-3}	5.52×10^{-3}
75%	5.29×10^{-4}	3.22×10^{-3}	1.16×10^{-2}	2.20×10^{-2}	2.28×10^{-2}
85%	7.68×10^{-4}	3.49×10^{-3}	1.84×10^{-2}	2.60×10^{-2}	4.50×10^{-2}
93%	9.93×10^{-4}	4.18×10^{-3}	2.30×10^{-2}	5.55×10^{-2}	5.67×10^{-2}
98%	3.19×10^{-3}	9.54×10^{-3}	2.45×10^{-2}	5.81×10^{-2}	8.24×10^{-2}

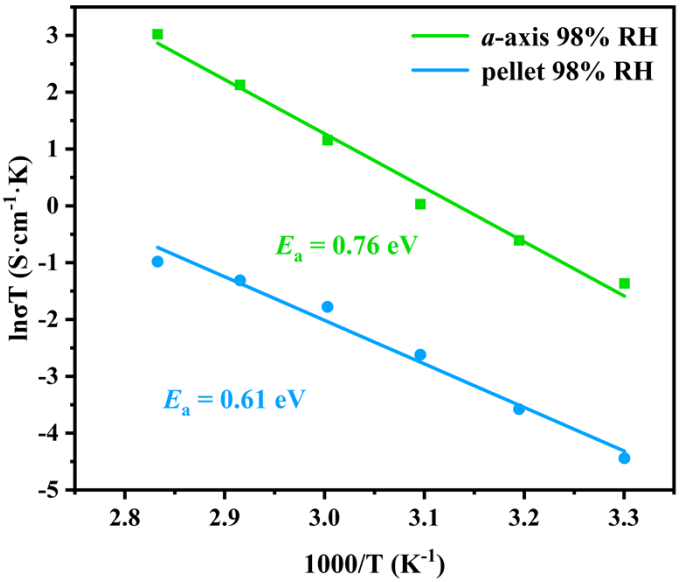

Figure S31. Arrhenius diagram of **iHOF-44** pellet and single crystal along the *a*-axis at 98% RH.

Section S9. Cyclic testing of proton conductivity of iHOFs.

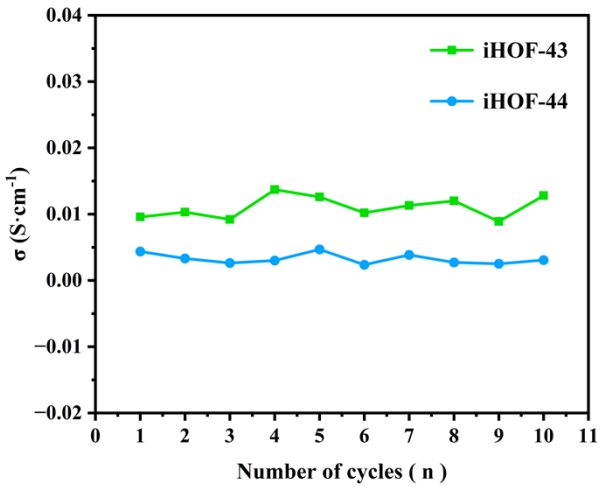

Figure S32. Results of iHOFs sample cycling tests.

Section S10. Comparison of Single-Crystal proton conductivity.

Table S5. Comparison of some typical Single-Crystal proton conductivity in some reported conducting materials.

Compound	Proton conductivity ($S \cdot cm^{-1}$)	Conditions	References
iHOF-16	0.388 [*a*-axis]	80ºC, 98%RH	[6]
	5.56×10^{-3} [*b*-axis]		
	3.25×10^{-4} [*c*-axis]		
	2.11×10^{-2} [pellet]	100ºC, 98%RH	
UPC-H9	0.237 [001]	80ºC, 60%RH	[7]
	2.44×10^{-3} [010]		
	7.13×10^{-3} [100]		
	6.39×10^{-2} [pellet]	80ºC, 80%RH	
UPC-H8	0.19 [001]	80ºC, 60%RH	
	1.28×10^{-3} [010]		
	5.04×10^{-3} [100]		
	3.09×10^{-2} [pellet]		
UPC-H5a@$NH_3 \cdot H_2O$	1.67×10^{-1} [001]	80ºC, 99%RH	[8]
	6.88×10^{-3} [100]		
	1.59×10^{-1} [pellet]		
GH–PMo_{12}	0.19 [001]	85ºC, 98%RH	[9]
	$1.06\times10^{-3}\perp$ [001]		
	6.04×10^{-3} [pellet]		
iHOF-43	1.66×10^{-1}[*a*-axis]	90ºC, 98%RH	This work
	5.67×10^{-3}[*b*-axis]		
	4.24×10^{-4}[*c*-axis]		
	1.25×10^{-2}[pellet]	100ºC, 98%RH	
iHOF-44	8.24×10^{-2}[*a*-axis]	90ºC, 98%RH	This work

	2.71×10^{-3}[pellet]	**100ºC, 98%RH**	
CPM-103a	**5.8×10^{-2} [SC]**	**22.5ºC, 98%RH**	**[10]**
	6.5×10^{-3} [pellet]		
CPM-103b	**4.8×10^{-2} [SC]**		
	5.9×10^{-3} [pellet]		
CB [6]·$1.2H_2SO_4$·$6.4H_2O$	**4.3×10^{-2} [001]**	**25ºC, 98%RH**	**[11]**
	1.3×10^{-3} [pellet]		
CB [6]·1.1HCl·$11.3H_2O$	**2.4×10^{-2} [001]**	**25ºC, 98%RH**	
	1.1×10^{-3} [pellet]		
[Pt_2(MPC)$_4Cl_2$ Co (DMA) (HDMA) guest]$_n$	**2.2×10^{-2} [010]**	**60ºC, 95%RH**	**[12]**
	2.7×10^{-4} [100]	**25ºC, 95%RH**	
	1.8×10^{-4} [001]		
	7.1×10^{-3} [pellet]	**60ºC, 95%RH**	
NNU-6	**1.91×10^{-2} [*a*-axis]**	**50ºC, 98%RH**	**[13]**
	2.42×10^{-4} [*b*-axis]		
	8.9×10^{-5} [*c*-axis]		
	1.21×10^{-3} [pellet]		
[(CN_3H_6)$_2$($C_{10}O_8H_4$)]	**1.78×10^{-2} [100]**	**25ºC, 98%RH**	**[14]**
	3.06×10^{-7} [010]		
	1.98×10^{-5} [001]		
	2.83×10^{-3} [pellet]	**85ºC, 98%RH**	
Pb-BSDC	**1.71×10^{-2} [long axis]**	**90ºC, 85%RH**	**[15]**
	1.43×10^{-4} [pellet]	**90ºC, 90%RH**	
[Pt(dach)(bpy)Br]$_4$(SO_4)$_4$·$32H_2O$	**1.7×10^{-2} [100]**	**55°C, 95%RH**	**[16]**
CFOS-1	**1.4×10^{-2} [SC]**	**25ºC, 98%RH**	**[17]**
	1.9×10^{-4} [pellet]	**50ºC, 98%RH**	
[In(imdcH)-(ox)] (NH_4)	**1.1×10^{-2} [SC]**	**22.5ºC, 98.5%RH**	**[18]**

$(H_2O)_{1.5}$	0.8×10^{-3} [pellet]	23.5ºC, 98.6%RH	
1-H_2O	1.2×10^{-2} // [001]	95ºC, 98%RH	[19]
	1.1×10^{-7} ⊥ [001]		
Co-MOF-74	1.2×10^{-2} // [*c*-axis]	25ºC, 92%RH	[20]
	1.2×10^{-3}⊥[*c*-axis]		
L-H	1.5×10^{-3}⊥[*c*-axis]	80°C，98% RH	[21]
	1.5×10^{-4} [*c*-axis]		
$K(H_2O)_6[M_6(btp)_6(H_2O)_{22}](P_2W_{18}O_{62})_3(Hbtp)_5(btp)_3\cdot52H_2O$ [M = Mn]	6.39×10^{-3} [001]	85ºC, 98% RH	[22]
	2.06×10^{-4}⊥ [001]		
	2.22×10^{-4} [pellet]		
$[Na_2(pytet)(Hdat)_2(H_2O)_3]\cdot2H_2O$	1.04×10^{-4} [100]	65ºC, 90% RH	[23]
	3.72×10^{-5}S [011]		
	4.03×10^{-6} [$0\bar{1}1$]		
	9.44×10^{-5} [pellet]		
MFM-722(Pb)-H_2O	6.61×10^{-4} [*c*-axis]	50ºC, 98% RH	[24]

Section S11. References.

1. S. Nandi, D. Chakraborty and R Vaidhyanathan, *Chem Comm*., 2016, **52**, 7249-7252.
2. M. Morshedi, M. Thomas, A. Tarzia, C. J. Doonan and N. G. White, *Chem. Sci*., 2017, **8**, 3019-3025.
3. X.-T. Bai, L.-H. Cao, C. Ji, F. Zhao, X.-Y. Chen, X.-J. Cao and M.-F. Huang, *Chem. Mater*., 2023, **35**, 3172-3180.
4. O. V. Dolomanov, L. J. Bourhis, R. J. Gildea, J. A. K. Howard and H. Puschmann, *J. Appl. Crystallogr.*, 2009, **42**, 339-341.
5. G. M. Sheldrick, *Acta Crystallogr C*., 2015, **71**, 3-8.
6. X.-J. Cao, L.-H. Cao, X.-T. Bai, X.-Y. Hou and H.-Y. Li, *Adv. Funct. Mater*., 2024, **34**, 2409359.
7. Y. Wang, M. Zhang, Q. Yang, J. Yin, D. Liu, Y. Shang, Z. Kang, R. Wang, D. Sun and J. Jiang, *Chem Comm*., 2020**, 56**, 15529-15532.
8. Y. Wang, J. Yin, D. Liu, C. Gao, Z. Kang, R. Wang, D. Sun and J. Jiang, *J. Mater. Chem. A*., 2021, **9**, 2683-2688.
9. M.-M. Wang, J.-J. Cai, H.-J. Lun, M.-G. Lv, J.-Q. Zhang, S. Andra, B.-B. Li, D.-B. Dang, Y. Bai, Y.-M. Li, *Adv. Funct. Mater.,* 2024, **34**, 2311912.
10. Q.-G. Zhai, C. Mao, X. Zhao, Q. Lin, F. Bu, X. Chen, X. Bu and P. Feng, *Angew. Chem. Int. Ed*., 2015, **54**, 7886-7890.
11. M. Yoon, K. Suh, H. Kim, Y. Kim, N. Selvapalam and K. Kim, *Angew. Chem. Int. Ed*., 2011, **50**, 7870-7873.
12. K. Otsubo, S. Nagayama, S. Kawaguchi, K. Sugimoto and H. Kitagawa, *JACS Au*., 2022, **2**, 109-115.
13. X.-L. Cao, S.-L. Xie, S.-L. Li, L.-Z. Dong, J. Liu, X.-X. Liu, W.-B. Wang, Z.-M. Su, W. Guan and Y.-Q. Lan, *Chem. Eur. J*., 2018, **24**, 2365-2369.
14. W.-W. Wu, B. Li, M.-M. Wang, J.-J. Cai, S. Andra, H.-J. Lun, Y. Bai, D.-B. Dang and Y.-M. Li, *Chem. Mater*., 2023, **35**, 6549-6556.
15. H. Zhang, Z.-A. Yan, Z.-M. Wu, Z.-Q. Lin, W.-M. Liao and J. He, *J. Solid State*

Chem., 2020, **287**, 121325.

16. K. I. Otake, K. Otsubo, T. Komatsu, S. Dekura, J. M. Taylor, R. Ikeda, K. Sugimoto, A. Fujiwara, C.-P. Chou, A. W. Sakti, Y. Nishimura, H. Nakai and H. Kitagawa, *Nat. Commun*.**,** 2020, **11**, 843.
17. C. Wang, T. Yan, G. Xing, S. Bailey, C. Lambert, P. Fayon, A. Trewin and T. Ben, *J. Solid State Chem*., 2022, **308**, 122903.
18. X. Zhao, C. Mao, X. Bu and P. Feng, *Chem. Mater*., 2014, **26**, 2492-2495.
19. M.-Y. Zhou, H.-Y. Wang, Z.-S. Wang, X.-W. Zhang, X. Feng, L.-Y. Gao, Z.-C. Lian, R.-B. Lin and D.-D. Zhou, *Chem Comm*., 2022, **58**, 771-774.
20. A. Javed, I. Strauss, H. Bunzen, J. Caro and M. Tiemann, *Nanomaterials*., 2020, **10**, 1263.
21. Y. Y. Sun, J. Wei, Z. H. Fu, M. Y. Zhang, S. E. Zhao, G. Xu, C. S. Li, J. Zhang and T. H. Zhou, *Adv. Mater.,* 2023, 35, 2208625.
22. L.-L. Chen, Y.-Y. Wu, W.-W. Wu, M.-M. Wang, H.-J. Lun, D.-B. Dang, Y. Bai and Y.-M. Li, *Inorg. Chem*., 2022, **61**, 8629-8633.
23. W.-W. Wu, J.-J. Cai, X.-Y. Liang, Z.-Z. Li, S. Andra, K. Gao, H.-J. Lun and Y.-M. Li, *ACS Appl. Mater*., 2024, **16**, 68358-68367.
24. X. Chen, Z. Y. Zhang, J. Chen, S. Sapchenko, X. Han, I. Da-Silva, M. Li, I. J. Vitorica-Yrezabal, G. Whitehead, C. C. Tang, K. Awaga, S. H. Yang and M. Schröder, *Chem Comm*., 2021, **57**, 65-68.